Vol. 565: 17–33, 2017
doi: 10.3354/meps12025

MARINE ECOLOGY PROGRESS SERIES
Mar Ecol Prog Ser

Published February 17

Iron availability modulates the effects of future CO_2 levels within the marine planktonic food web

María Segovia[1,*], M. Rosario Lorenzo[1], María T. Maldonado[2], Aud Larsen[3], Stella A. Berger[4,5], Tatiana M. Tsagaraki[4], Francisco J. Lázaro[6], Concepción Iñiguez[1], Candela García-Gómez[1,9], Armando Palma[1], Michaela A. Mausz[7,10], Francisco J. L. Gordillo[1], Jose A. Fernández[8], Jessica L. Ray[3], Jorun K. Egge[4]

[1]Department of Ecology, Faculty of Sciences, University of Málaga, Bulevar Louis Pasteur s/n, 29071 Málaga, Spain
[2]Department of Earth and Ocean and Atmospheric Sciences, University of British Columbia, 2207 Main Mall, Vancouver, BC V6T 1Z4, Canada
[3]Uni Research Environment and Hjort Centre for Marine Ecosystem Dynamics, Thormøhlensgt 41, 5006 Bergen, Norway
[4]Department of Biology, Thormøhlensgt 53A/B, University of Bergen, 5020 Bergen, Norway
[5]Department of Experimental Limnology, Leibniz-Institute of Freshwater Ecology and Inland Fisheries (IGB), Alte Fischerhütte 2, 16775 Stechlin, Germany
[6]Department of Science and Technology of Materials and Fluids, University of Zaragoza, María de Luna 3, 50018 Zaragoza, Spain
[7]Institute of Inorganic and Analytical Chemistry/Bioorganic Analytics, Friedrich Schiller University Jena, 07743 Jena, Germany
[8]Department of Plant Biology, Faculty of Sciences, University of Málaga, Bulevar Louis Pasteur s/n, 29071 Málaga, Spain
[9]*Present address:* Spanish Oceanographic Institute (IEO), Puerto Pesquero, 29640 Fuengirola, Málaga, Spain
[10]*Present address:* School of Life Sciences, University of Warwick, Coventry CV4 7AL, UK

ABSTRACT: Ocean acidification (OA) due to increased anthropogenic CO_2 emissions is affecting marine ecosystems at an unprecedented rate, altering biogeochemical cycles. Direct empirical studies on natural communities are required to analyse the interactive effects of multiple stressors while spanning multiple trophic levels. We investigated the interactive effects of changes in CO_2 and iron availability on functional plankton groups. We used mesocosms manipulating the carbonate system from the start to achieve present (low concentration, LC) and predicted future pCO_2 levels (high concentration, HC). To manipulate dissolved iron (dFe), half of the mesocosms were amended with 70 nM (final concentration) of the siderophore desferoxamine B (DFB) on Day 7 (+DFB and −DFB treatments). Manipulation of both CO_2 and DFB increased dFe compared to the control. During the 22 experimental days, the plankton community structure showed 2 distinct phases. In phase 1 (Days 1–10), only bacterioplankton abundances increased at elevated pCO_2. In contrast, a strong community response was evident in phase 2 (Days 11–22) due to DFB addition. Biomass of the coccolithophore *Emiliania huxleyi* increased massively at LC+DFB. HC negatively affected *E. huxleyi* and *Synechococcus* sp., and high dFe (+DFB) had a positive effect on both. The rest of the plankton community was unaffected by the treatments. Increased dFe partially mitigated the negative effect of HC imposed on the coccolithophores, indicating that *E. huxleyi* was able to acclimate better to OA. This physiological iron-mediated acclimation can diminish the deleterious effects of OA on carbon export and the rain ratio, thus affecting food web dynamics and future ecosystem functioning.

KEY WORDS: Global change · Iron · CO_2 · Mesocosms · Plankton food web · *Emiliania huxleyi* · *Synechococcus* sp.

*Corresponding author: segovia@uma.es

INTRODUCTION

In the geological past, planet Earth has experienced significant changes in natural climate-driven factors. At present, the main drivers such as carbon dioxide (CO_2) concentration, eutrophication and ultraviolet radiation are increasing at an unprecedented rate (Hoegh-Guldberg & Bruno 2010). The level of CO_2 in the atmosphere is projected to reach a partial pressure of 900 µatm (or a concentration of 900 ppmv) by the end of this century (Stocker et al. 2013). This will alter seawater chemistry by lowering its pH (ocean acidification, OA) and the saturation state of calcium carbonate (Doney et al. 2009). Within plankton, phytoplankton play key roles in biogeochemical cycles, in marine food web dynamics and productivity, as well as in the consumption and production of greenhouse gases. Changes in climate are likely to affect phytoplankton productivity and species composition (Riebesell & Tortell 2011). Increased CO_2 levels within future scenarios may benefit some phytoplankton species while being detrimental to others (Riebesell & Tortell 2011). Haptophytes (e.g. coccolithophores) are of global importance in the carbon cycle, but this phytoplankton phylum is most affected by elevated CO_2 concentration (Meyer & Riebesell 2015 and references therein). Additionally, carbonate chemistry may undergo greater changes in colder waters due to the higher solubility of CO_2 at lower temperatures (Riebesell et al. 2013). While coccolithophore abundance strongly declines south of the Polar Frontal Zone and blooms are not formed in the Southern Ocean (Malinverno et al. 2015), coccolithophores do typically bloom in high-latitude areas such as the Arctic (Dylmer et al. 2015). Experimental work on the effects of high pCO_2 on coccolithophores has revealed contradictory results depending on the species and strain used, the physico-chemical conditions, and whether the studies were carried out in natural communities or with laboratory cultures (Langer et al. 2006, Hutchins 2011, Riebesell & Tortell 2011, Mackey et al. 2015). Furthermore, the impact of elevated pCO_2 on organisms in other trophic levels is not well understood. Studies focusing on micro- and mesozooplankton, bacterioplankton or viruses have yielded results that are often contradictory and/or inconclusive (Larsen et al. 2008, Caron & Hutchins 2013, Niehoff et al. 2013, Calbet et al. 2014, Endres et al. 2014).

OA affects marine nutrient biogeochemistry and, in particular, has a profound impact on trace metal solubility and speciation (Millero et al. 2009). Among metals, Fe is the most essential micronutrient controlling phytoplankton growth mainly, but not exclusively, through nitrate assimilation and photosynthesis (Behrenfeld & Milligan 2013). Fe bioavailability, i.e. iron available for uptake, and therefore growth, is controlled by many factors including (1) dissolved Fe concentrations; (2) the concentration and strength of iron-binding organic ligands (OLs) which modulate Fe speciation; (3) irradiance, which affects iron redox chemistry and ligand binding strength; and (4) pH, which greatly influences the chemistry of metals in seawater (Sunda & Huntsman 1995, Maldonado & Price 2001, Barbeau et al. 2003, Shi et al. 2010). Low pH increases Fe solubility and thus enhances dissolved iron (dFe) concentrations (Millero et al. 2009). Similarly, elevated CO_2 enhanced dFe levels during a mesocosm experiment in a Norwegian fjord (Breitbarth et al. 2010b) and in subarctic waters (Yoshimura et al. 2013). However, the effects of OA on organically bound iron are more complex and affect Fe bioavailability. Organic ligands solubilise particulate iron and increase the residence time of dFe in the ocean. Depending on the Fe ligand type (carboxylates, hydroxymates or cathecholates) the bioavailability of Fe can either decrease or remain unaffected under OA (Shi et al. 2010). Thus, the net effect of OA on phytoplankton iron nutrition depends on the balance between increase in iron solubility and changes in iron bioavailability mediated by organic ligand complexation.

In a rapidly changing environment, it is critical to gain adequate understanding of the vulnerability of ecosystems to globally driven perturbations. However, predictions for whole ecosystems are challenging because of synergistic and antagonistic effects of multiple stressors (Crain et al. 2008). Perturbation studies in natural communities using *in situ* mesocosms are necessary to address such challenges, because of their high degree of realism compared to microcosms, and the impracticability of performing large-scale OA experiments in the open ocean (in which mechanistic relationships are not always identified) (Stewart et al. 2013). Specifically, mesocosm experiments allow direct analysis of the interactive effects of multiple stressors across multiple trophic levels (Riebesell et al. 2010, Stewart et al. 2013, Riebesell & Gattuso 2015).

Here we present the main results from a mesocosm experiment that aimed to investigate the effects of future changes in pCO_2 and Fe availability during a bloom of the coccolithophore *Emiliania huxleyi* within a natural plankton community. *E. huxleyi* is a major primary producer in the world's oceans and is sensitive to elevated pCO_2. This phytoplankton species is of paramount significance in the global carbon cycle. *E. huxleyi* is responsible for a large fraction of the ocean calcium carbonate production and export

to the deep ocean and contributes to the regulation of the exchange of CO_2 across the ocean–atmosphere interface through the rain ratio (Rost & Riebesell 2004). To our knowledge, this mesocosm experiment is the first to manipulate pCO_2 and iron concentrations simultaneously, and examine their single and combined effects on the plankton food web and the interactions of planktonic organisms within multiple trophic levels.

We investigated (1) the effects of elevated pCO_2 levels on dissolved Fe; (2) the extent to which changes in Fe availability affect the growth of *E. huxleyi* and other autotrophs; and (3) whether different pCO_2 and Fe levels, and their interaction, lead to cascading effects on other members of the plankton community.

MATERIALS AND METHODS

Experimental design

A mesocosm experiment was carried out in the Raunefjord (60.39° N, 5.32° E) off Bergen, Norway, from 5 to 27 June 2012. Twelve mesocosms (11 m^3 each) were set up in a full factorial design with all combinations of ambient and high pCO_2 and 2 treatments of dFe in 3 independent replicate mesocosms per treatment. High-density polyethylene (HDPE) mesocosms were filled with fjord water pumped from 8 m depth. They were covered with low-density polyethylene (LDPE) lids in order to avoid CO_2 losses and contamination. Mesocosms and their lids were transparent to photosynthetically active radiation (PAR) and ultraviolet radiation (UVR). After the first sampling day (Day 0), the seawater of half of the mesocosms was enriched with CO_2 (Schulz et al. 2009) to achieve pCO_2 concentrations corresponding to levels predicted for the year 2100 (900 µatm, high concentration: HC) (Stocker et al. 2013) while the other half was not manipulated (ca. 390 µatm, low concentration: LC). All mesocosms were continuously and gently mixed by using an airlift system (Egge & Heimdal 1994). For the CO_2 enrichment, 150 l of fjord water was aerated with pure CO_2 at a flow rate of 1.5 l min^{-1} overnight and added to each of the high pCO_2 (HC) mesocosms. To maintain the pCO_2 in the HC treatments, ambient air was mixed with pure CO_2 at a flow rate of 200 ml min^{-1}, and the enriched mixture (900 µatm CO_2) was pumped directly to the airlift system. The LC treatment consisted of only ambient air similarly connected. HEPA filters were placed between the air pumps and the airlift system to avoid particulate contamination. Mesocosms were fertilised after initial sampling (Day 0) by addition of 10 µM nitrate and 0.3 µM phosphate to induce a bloom of the coccolithophore *Emiliania huxleyi* (Egge & Heimdal 1994). To induce changes in Fe availability, and analyse its effects on the plankton community, 70 nM (final concentration) of the siderophore desferrioxamine B (DFB) (+DFB and –DFB treatments) was added to half of the mesocosms on Day 7, when the community was already acclimated to high CO_2. The initial dFe concentration before DFB addition was about 4.5 nM. Even though DFB is a strong Fe-binding organic ligand often used to induce iron limitation in phytoplankton (Wells 1999), DFB additions may also increase the dissolved Fe pool in environments with high concentrations of colloidal and/or particulate Fe, such as fjords (Kuma et al. 1996, Öztürk et al. 2002). The multifactorial treatments were named LC–DFB (control), LC+DFB, HC+DFB and HC–DFB. Water samples from each mesocosm were taken from 2 m depth by gentle vacuum pumping of 25 l volume into acid-washed carboys that were quickly transported to the onshore laboratory. All variables were analysed on a daily basis and/or every other day, except where otherwise stated.

pCO_2, DIC, $\Omega_{calcite}$, pH, alkalinity and rain ratio

pCO_2 inlet flow in each mesocosm was measured by non-dispersive infrared analysis by using a CO_2 gas analyser (LI-820, Li-COR). pCO_2, dissolved inorganic carbon (DIC) and the calcite saturation state ($\Omega_{calcite}$) were calculated from daily measurements of pH, temperature, salinity and total alkalinity (TA) using the CO_2Calc software (Robbins et al. 2010). pH was measured in all mesocosms using a pH meter (CRISON Basic 20+) calibrated daily using the National Bureau of Standards scale. Salinity was measured with a conductivity meter (CRISON 524). The accuracy of the pH meter and conductivity meter was ±0.01 pH units and ±1.5 %, respectively. TA was measured using the classical Gran's potentiometric method (Gran 1952). The rain ratio (RR, the ratio of particulate inorganic to organic carbon in exported biogenic matter), was calculated applying the models of Ridgwell et al. (2007) and Hofmann & Schellnhuber (2009).

Dissolved iron (dFe)

Water samples to measure dFe were obtained from each mesocosm every fourth day starting on Day 6 of

the experiment. Samples were filtered through 0.2 µM AcroPak supor membrane capsule filters (Pall) into LDPE bottles, and immediately acidified with ultra-clean HCl (Seastar) in a Class 100 laminar flow hood. Total dFe measurements were conducted by chemiluminescence flow injection analysis (CL-FIA, Waterville Analytical) as described by de Baar et al. (2008) and de Jong et al. (1998). All filters, sampling and filtration equipment were trace metal cleaned using HCl and subsequent high purity water (MilliQ) rinses and protected with double bags for storage and transport. Total iron concentration (see Fig. S2 in the Supplement at www.int-res.com/articles/suppl/m565p017_supp.pdf) consists of both dissolved and particulate iron pools (dFe and PFe). Particulate iron analyses are described in Methods S1 in the Supplement. Trace metal clean techniques were used throughout all processes, when cleaning all material used before sampling, and when collecting and manipulating samples for both dissolved and particulate metals analyses.

Inorganic and organic nutrients

Inorganic nutrient concentrations were analysed in a QuAAtro AQ2 AACE autoanalyser (Seal Analytical) following the methods described by Grashoff et al. (1983). Water samples (50 ml) from each mesocosm were collected every other day, filtered through 0.7 µm GF filters (Millipore) and immediately frozen at –20°C until analysis. The detection limits of the inorganic nutrients were 0.03 µM for nitrate, 0.01 µM for nitrite, 0.02 µM for phosphate, 0.05 µM for silicic acid and 0.06 µM for ammonia. Dissolved organic carbon (DOC) and nitrogen (DON) were analysed from 50 ml water samples, collected every other day, filtered through 0.2 µm cellulose acetate filters (Whatman) and stored in acid-washed and precombusted glass bottles at 4°C in darkness until analysis. DOC and total dissolved nitrogen (TDN) were measured in a Shimadzu TOC-L analyser equipped with a total nitrogen module (TNM-1). DON was calculated by subtracting the total inorganic nitrogen fraction from TDN.

Chlorophyll *a* (chl *a*) concentration and *in vivo* chl *a* fluorescence

Water samples (750 ml) were collected every other day from each mesocosm to determine total chl *a* concentration. Samples were filtered onto 0.7 µm GF filters (Millipore) and kept at –80°C until analyses. Chl *a* was extracted in N,N-dimethylformamide overnight at 4°C in the dark. Chl *a* content was determined spectrophotometrically, and the concentrations were calculated by using equations from Wellburn (1994). Optimal quantum yield (F_v/F_m) of Photosystem II (PSII) charge separation was measured in 10 min dark-adapted samples by pulse amplitude modulated fluorometry (Water-PAM, Waltz) as described by Schreiber et al. (1986). After initial dark measurement and a saturation pulse to determine minimum fluorescence (F_0) and maximum fluorescence (F_m), respectively, F_v/F_m was obtained as $(F_m - F_0)/F_m$. Thus, F_v is the maximal variable fluorescence of a dark-adapted sample, F_m is the maximal fluorescence intensity with all PSII reaction centres closed, and F_0 is the basal fluorescence. High F_v/F_m values indicate that cells are in healthy physiological condition, whereas a decrease in F_v/F_m indicates cell stress (Foyer et al. 1994, Behrenfeld & Milligan 2013).

Plankton analyses

Phytoplankton <20 µm and bacterioplankton

Phytoplankton cells smaller than 20 µm from each mesocosm were analysed using a FACSCalibur flow cytometer (Becton Dickinson) equipped with an air-cooled laser providing 15 mW at 488 nm and with a standard filter set-up. The trigger was set on red fluorescence and samples were analysed for 300 s at an average flow rate of 56 µl min^{-1}. Autotrophic groups were discriminated on the basis of the side-scatter signal (SSC) versus pigment autofluorescence (chlorophyll and phycoerythrin) according to Marie et al. (1999) and Larsen et al. (2001). Abundances were converted into carbon biomass according to Kana & Glibert (1987), Menden-Deuer & Lessard (2000) and Olenina et al. (2006).

Enumeration of bacterioplankton was performed according to Marie et al. (1999). The samples were fixed with glutaraldehyde (0.5% final concentration) for 30 min at 4°C, snap frozen in liquid nitrogen, and stored at –80°C. Samples were stained with SYBR Gold Nucleic Acid Stain (Invitrogen) and counted by using a Cytomics FC 500 flow cytometer (Beckman Coulter) equipped with a 20 mW 488 nm air-cooled argon-ion laser and standard filters. The discriminator was set to green fluorescence and the samples were analysed for 60 s at a flow rate of 30 µl min^{-1}. Data were calibrated by measuring

latex fluorospheres (1.0 µm in diameter; Polysciences) at 525 nm using CXP analysis software. Bacterial abundances were transformed into carbon biomass according to Lee & Fuhrman (1987) and Vrede et al. (2002).

Phytoplankton >20 µm and microzooplankton

Live samples were immediately analysed with a FlowCAM (Fluid Imaging Technologies) using a 4× objective and a 300 µm flowcell to analyse particles ranging from 18 to 1000 µm equivalent spherical diameter (ESD) and run in automatic imaging mode (Jakobsen & Carstensen 2011). Aliquots (6.3 ml) of each sample were analysed at flow rates adjusted to guarantee that no more than 1 particle appeared in each frame. All image collages were post analysed to separate the main taxonomic groups (diatoms, dinoflagellates and ciliates). Abundances and particle sizes of these groups (Jakobsen & Carstensen 2011) were then converted into carbon biomass using the equations provided by Menden-Deuer & Lessard (2000).

Mesozooplankton

Mesozooplankton was sampled at the beginning and at the end of the experiment. At the beginning, samples were collected by filtering 2.2 m^3 water pumped through a 90 µm Apstein plankton net (Hydrobios) as described by Nejstgaard et al. (2006). At the end of the experiment, the whole water column of the mesocosms was mixed with a 45 cm disc (Striebel et al. 2013), immediately sampled by 2 vertical 90 µm net tows (3.85–0 m) and preserved in 4% borax-buffered formaldehyde solution. Species composition and abundance of each replicate within each treatment was determined using a dissecting microscope, and the total mesozooplankton biomass was calculated according to Nejstgaard et al. (2006).

Net growth rates

Apparent net growth rates for phytoplankton and bacterioplankton were calculated according to the logistic model:

$$\ln((K - N)/N) \quad (1)$$

where K refers to the loading capacity of the mesocosms, and N is the cell density at any given time.

Iron requirements

Fe demand (mol Fe l^{-1} of seawater) for each phytoplankton group was calculated using published Fe:C ratios (µmol Fe mol^{-1} C) and the maximum C biomass achieved by each phytoplankton group during the experiment. C biomasses were calculated as described above. We used published Fe:C ratios (µmol:mol) for *E. huxleyi* (Muggli & Harrison 1996), diatoms (Sarthou et al. 2005), *Synechococcus* and prasinophytes (Quigg et al. 2011), picoeukaryotes (Timmermans et al. 2005) and dinoflagellates (Marchetti & Maldonado 2016).

Irradiance and temperature

Solar spectral irradiance comprising PAR wavelengths (400–700 nm) ultraviolet A (UVA, 320–400 nm) and ultraviolet B (UVB, 280–320 nm) was recorded at 2 m depth in one mesocosm (5 min intervals) using a Ramses spectroradiometer (TrioS). Although the holding construction of the spectroradiometer was made of stainless steel, some screws developed a crust of ferric material, which interfered with all of the analyses. Thus, this mesocosm was excluded as a replicate and was only used for irradiance measurements. HOBO Pendant Temperature/Light loggers (Onset Computer) were attached to the airlift system in one replicate of each treatment at depths of 0, 1, 2 and 3 m to ensure that mesocosms received the same irradiance as well as to monitor water temperature.

Statistical analyses

Statistical significance of treatment effects on variables measured was analysed by performing split-plot ANOVAs (SPANOVAs, or mixed-model ANOVAs) followed by post hoc Sidak or Tukey and Bonferroni tests, respectively (considering $p < 0.05$ and/or $p < 0.01$ as significant). When appropriate, data were specifically tested for significant differences ($p < 0.05$) induced by the treatments by using 1- or 2-way ANOVAs and/or Student's *t*-tests, as well as Pearson's product-moment correlations. All analyses were performed using the general linear model (GLM) procedure with main effects (CO_2, dFe), time (repeated measure) and all interactions. Data were previously checked for normality (by Shapiro-Wilks' test), homoscedasticity (by Cochran's and Levene's tests) and sphericity (by Mauchly's and/or Bartlett's

tests). Variables met all criteria mentioned above. Statistical analyses were performed using the software Statistica v12 (Statsoft) and SPSS v22 (IBM statistics).

RESULTS

Experimentally induced stressors (carbonate system and dissolved iron)

The experimental set-up was partially successful in that pCO_2 reflected the level of 900 µatm in the high CO_2 treatment (HC) versus 390 µatm at initial times in the ambient CO_2 treatment (LC) (Fig. 1a). pCO_2 dropped significantly about 2-fold between Days 3 and 10 (Bonferroni, $p < 0.001$) as a consequence of biological activity in both HC and LC treatments, causing changes in pH. Re-addition of CO_2-enriched fjord water on Days 3, 7 and 10 (in HC) re-established pCO_2 to 1100 µatm and stabilised pH at around 7.8 in HC. However, in the LC treatments, pCO_2 was around 300 µatm during the experiment (except for Days 0 to 3), which was lower than our aimed ambient CO_2 level. This promoted oscillations in pH between 8.1 and 8.3 in LC treatments (Table 1). Average alkalinity was 2029 (±60 SD) µmol l^{-1} for all mesocosms, and DIC remained stable after Day 5 at 1953 (± 36) µmol l^{-1} in HC and 1795 (± 61) µmol l^{-1} in LC (Table 1). $\Omega_{calcite}$ was significantly higher in LC than in HC treatments (*t*-test $p < 0.05$; Table 1).

To induce changes in Fe availability, 70 nM of the siderophore DFB was added to half of the mesocosms. Contrary to expectations, the DFB addition increased dFe instead of promoting Fe limitation in this experiment. Before DFB was added on Day 7, the initial dFe concentration was 4.5 nM (mean of all mesocosms), without significant differences between LC and HC treatments (Fig. 1b, SPANOVA, $p = 0.069$). Dissolved Fe concentrations in the control (LC–DFB) remained at this level throughout the experiment (SPANOVA, $p = 0.399$, Bonferroni $p < 0.001$). The DFB amendment on Day 7 resulted in a significant ca. 3-fold increase in dFe in both HC and LC treatments by Day 17 (Sidak $p = 0.003$ and $p = 0.0004$, respectively) relative to the initial levels (Bonferroni $p = 0.002$). On Day 17, the only treatment significantly different from the rest in terms of dFe was the control, showing the lowest dFe levels (LC–DFB, Sidak $p = 0.0004$). At high pCO_2 without DFB addition (i.e. HC–DFB), dFe also increased ca. 3-fold by Day 17, confirming an increase in iron solubility due to lowering pH (Millero et al. 2009). Surprisingly, dFe decreased sharply between Days 17 and 21 in the HC–DFB treatment. In contrast, the +DFB treatments sustained high dFe throughout Day 21, regardless of the pCO_2 level (Sidak $p \leq 0.025$). These results suggest that Fe solubility was enhanced by either the addition of DFB and/or CO_2. Furthermore, significant effects of pCO_2, DFB and their interaction were observed in the availability of dFe during the experiment (all Sidak $p \leq 0.05$).

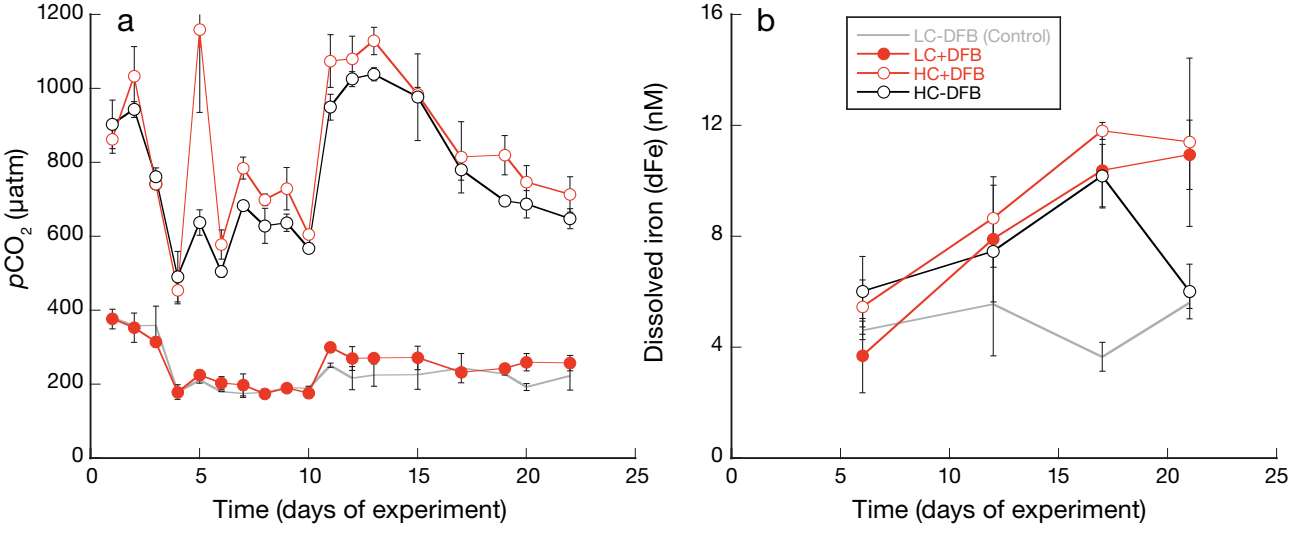

Fig. 1. Temporal development of (a) CO_2 partial pressure (pCO_2) and (b) dissolved iron (dFe) within the mesocosms. Ambient pCO_2 and ambient dFe (LC–DFB, grey); ambient pCO_2 and increased dFe (LC+DFB, red filled circle); increased pCO_2 and increased dFe (HC+DFB, red open circle), increased pCO_2 and ambient dFe (HC–DFB, black open circle). Symbols indicate means of measurements in 3 independent mesocosms (n = 3) except for LC–DFB where n = 2. Error bars indicate SD

Table 1. Measured pH, total alkalinity (TA, µmol l^{-1}), calculated dissolved inorganic carbon (DIC, µmol l^{-1}) and calcite saturation state ($\Omega_{calcite}$) under the different treatments; LC: ambient CO_2 (390 µatm); HC: increased CO_2 (900 µatm); –DFB (ambient dissolved iron, dFe); +DFB (increased dFe). Note that DFB was added on Day 7. Data are means (± SD) of 3 independent mesocosm bags, except for LC–DFB treatment in which n = 2. Significant differences between treatments within each day are represented by different superscript letters (2-way ANOVA followed by post hoc Tukey tests, where $p < 0.05$ is significant). The rain ratio (RR) was calculated applying the models from Ridgwell et al. (2007) and Hofmann & Schellnhuber (2009). The calculated RR represents the average between the 2 models, with SD in brackets

Variable	Day	Treatment			
		LC–DFB	LC+DFB	HC+DFB	HC–DFB
pH	1	8.04 (0.01)^{a}	8.05 (0.02)^{a}	7.71 (0.02)^{b}	7.70 (0.04)^{b}
	3	8.06 (0.05)^{a}	8.10 (0.02)	7.77 (0.01)^{b}	7.75 (0.01)^{b}
	5	8.24 (0.02)^{a}	8.22 (0.02)^{a}	7.66 (0.15)^{b}	7.81 (0.02)^{b}
	10	8.28 (0.01)^{a}	8.30 (0.03)^{a}	7.84 (0.00)^{b}	7.86 (0.01)^{b}
	22	8.22 (0.06)^{a}	8.16 (0.03)^{a}	7.77 (0.03)^{b}	7.81 (0.02)^{b}
TA	1	2100 (20)^{a}	2176 (40)^{a}	2096 (25)^{a}	2140 (34)^{a}
	3	2086 (23)^{a}	2046 (6)^{a}	2060 (35)^{a}	2046 (15)^{a}
	5	2027 (40)^{a}	2032 (8)^{a}	1956 (108)^{a}	1975 (67)^{a}
	10	2045 (48)^{a}	2006 (5)^{a}	2021 (14)^{a}	2013 (15)^{a}
	22	2003 (35)^{a}	1983 (38)^{a}	1996 (15)^{a}	2006 (12)^{a}
DIC	1	1933 (6)^{a}	2002 (44)^{ab}	2041 (20)^{bc}	2086 (25)^{c}
	3	1910 (33)^{a}	1861 (11)^{a}	1989 (33)^{b}	1980 (16)^{b}
	5	1775 (27)^{a}	1793 (14)^{a}	1917 (143)^{a}	1894 (66)^{a}
	10	1769 (34)^{a}	1727 (17)^{a}	1915 (16)^{b}	1930 (14)^{b}
	22	1777 (38)^{a}	1773 (28)^{a}	1926 (7)^{b}	1924 (10)^{b}
$\Omega_{calcite}$	1	2.98 (0.04)^{a}	3.15 (0.10)^{a}	1.50 (0.08)^{b}	1.53 (0.14)^{b}
	3	3.07 (0.25)^{a}	3.28 (0.09)^{a}	1.68 (0.04)^{b}	1.63 (0.04)^{b}
	5	4.16 (0.50)^{a}	4.22 (0.15)^{a}	1.30 (0.60)^{b}	1.77 (0.09)^{b}
	10	4.49 (0.03)^{a}	4.85 (0.21)^{a}	1.93 (0.01)^{b}	2.01 (0.02)^{b}
	22	4.08 (0.30)^{a}	3.59 (0.29)^{a}	1.64 (0.10)^{b}	1.80 (0.07)^{b}
RR	1	0.75 (0.06)^{a}	0.80 (0.08)^{a}	0.41 (0.11)^{b}	0.41 (0.10)^{b}
	3	0.77 (0.07)^{a}	0.82 (0.08)^{a}	0.45 (0.09)^{b}	0.44 (0.09)^{b}
	5	1.06 (0.19)^{a}	1.03 (0.18)^{a}	0.38 (0.10)^{b}	0.47 (0.08)^{b}
	10	1.15 (0.25)^{a}	1.21 (0.29)^{a}	0.51 (0.07)^{b}	0.53 (0.06)^{b}
	22	1.03 (0.18)^{a}	0.90 (0.11)^{a}	0.44 (0.09)^{b}	0.48 (0.08)^{b}

Inorganic and organic nutrients

Nitrate decreased 15-fold from Days 1 to 7 below the detection limits, and there were no differences due the treatments (i.e. HC vs. LC) except for Day 1 when LC was higher than HC with 7.44 and 5.90 µM nitrate, respectively (Fig. 2a, Sidak $p = 0.032$; Bonferroni $p < 0.001$). Ammonium concentration increased significantly between Days 5 and 15 (Fig. 2b, Bonferroni $p = 0.002$) independent of treatments. Silicic acid concentration was low from the beginning (average 0.6 µM; Fig. 2c) and showed no differences between treatments (all SPANOVA, $p > 0.05$). Soluble reactive phosphate was below the detection limit from the beginning of the experimental period (Fig. 2d). DOC remained constant between 1.18 and 2 mg ml^{-1} (Fig. 2e) without differences between treatments. DON sharply increased about 3-fold on Day 5 in all mesocosms (Fig. 2f, Bonferroni $p = 0.006$), decreased immediately after and then remained stable at ca. 1 mg l^{-1}.

Plankton community structure and dynamics

The experiment was divided in 2 clearly different phases, indicated by significant changes in chl *a* and the carbon-based biomass of plankton groups (Figs. 3 & 4). Phase 1 comprised Days 0 to 10, and phase 2 was Days 11 to 22.

In phase 1, chl *a* decreased from 4.34 to 0.87 µg l^{-1} in all mesocosms (Fig. 3a) due to the rapid break-down of a diatom bloom (also in the fjord), which was dominated by chain-forming *Skeletonema* sp. (Fig. 4f, Fig. S1f in the Supplement). Picoeukaryotes (0.1–2 µm), small nanoeukaryotes (2–7 µm), large nanoeukaryotes (6–20 µm) and dinoflagellates (20–200 µm) showed comparable peak dynamics and declined towards the end of phase 1 (Fig. 4c–e,g). This decline was followed by similar dynamics in the ciliate community (Bonferroni $p < 0.001$; Fig. 4h, Fig. S1). There were no significant differences between treatments in chl *a* and F_v/F_m (Fig. 3) nor for any of the planktonic groups (Fig. 4, all SPANOVA, $p > 0.05$) during phase 1. Only heterotrophic bacterioplankton biomass (Fig. 4i) and its net growth rate were significantly higher in the HC treatment compared to the LC treatment by Days 9 to 10 (~64 µg C l^{-1}, post hoc Sidak $p = 0.026$ and $p = 0.016$, Days 9 and 10, respectively). However, biomass and net growth rates of bacterioplankton reversed and were higher in the LC than HC treatments during phase 2 (Table 2).

During phase 2, chl *a* concentration increased in all treatments (Fig. 3a) due to elevated biomass of *Emiliania huxleyi* (5–10 µm), *Synechococcus* (0.6–2 µm), small and large nanoeukaryotes and, to a lesser extent, dinoflagellates (20–200 µm; Fig. 4a–e, g). Chl *a*

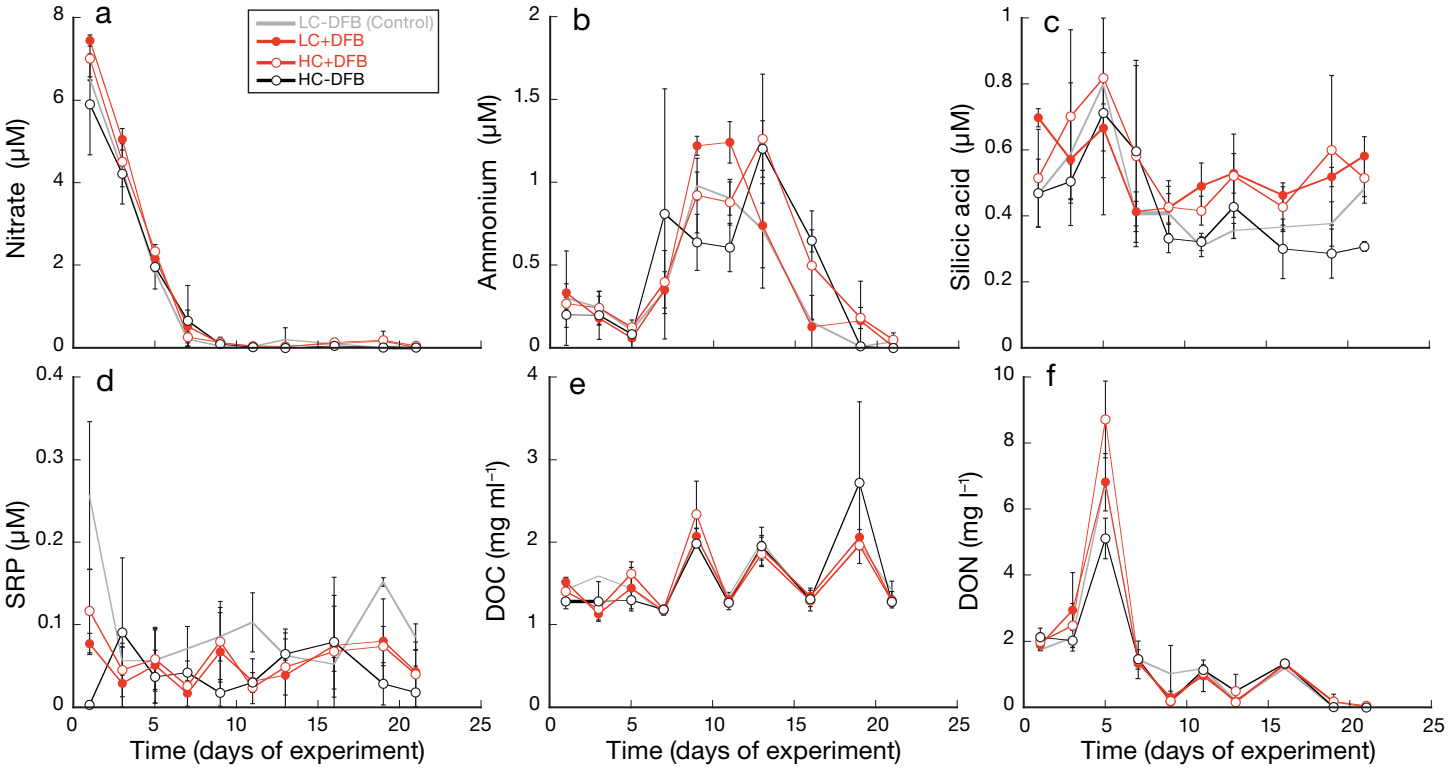

Fig. 2. Temporal development of major nutrient concentrations within the mesocosms in the different treatments: (a) nitrate, (b) ammonium, (c) silicic acid, (d) soluble reactive phosphate (SRP), (e) dissolved organic carbon (DOC), (f) dissolved organic nitrogen (DON). Symbols as in Fig. 1

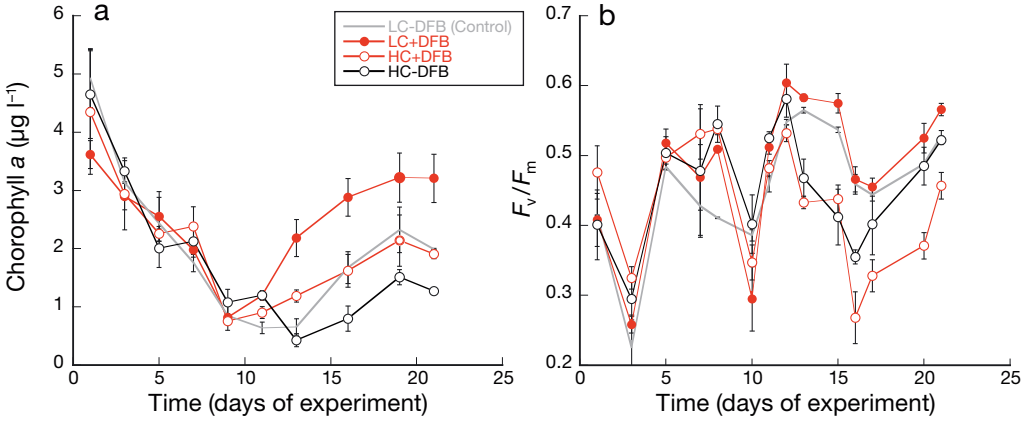

Fig. 3. Temporal development of (a) total chl *a* concentration and (b) optimal quantum yield of chl *a* associated with photosystem II (F_v/F_m) within the mesocosms in the different treatments. Symbols as in Fig. 1

remained below 2 µg l^{-1} in the HC treatments, while it culminated at ~3.5 µg l^{-1} on Day 19 under LC+DFB conditions (Fig. 3a). Significant differences in chl *a* concentration between HC and LC were observed independent of DFB addition (Fig. 3a; Tukey $p < 0.0001$). However, DFB addition (on Day 7) had a delayed positive effect on chl *a* in phase 2 (Tukey $p < 0.0001$ and Bonferroni $p \leq 0.001$). F_v/F_m was significantly higher in LC than in HC treatments in this period (Fig. 3b; $p < 0.05$). Under LC conditions, +DFB promoted a significant increase in F_v/F_m with respect to the control (LC–DFB; Fig. 3b, Sidak $p < 0.05$). In contrast, in the HC treatments, F_v/F_m was higher in the absence of DFB. The coccolithophore *E. huxleyi* and the cyanobacterium *Synechococcus* sp. were affected by both pCO_2 and Fe conditions.

A massive increase in *E. huxleyi* biomass was evident in the LC+DFB treatment, reaching 1600 µg C l^{-1} corresponding to 60 000 cells ml^{-1} in phase 2 (Fig. 4a and Fig. S1a, respectively). In contrast, *E.*

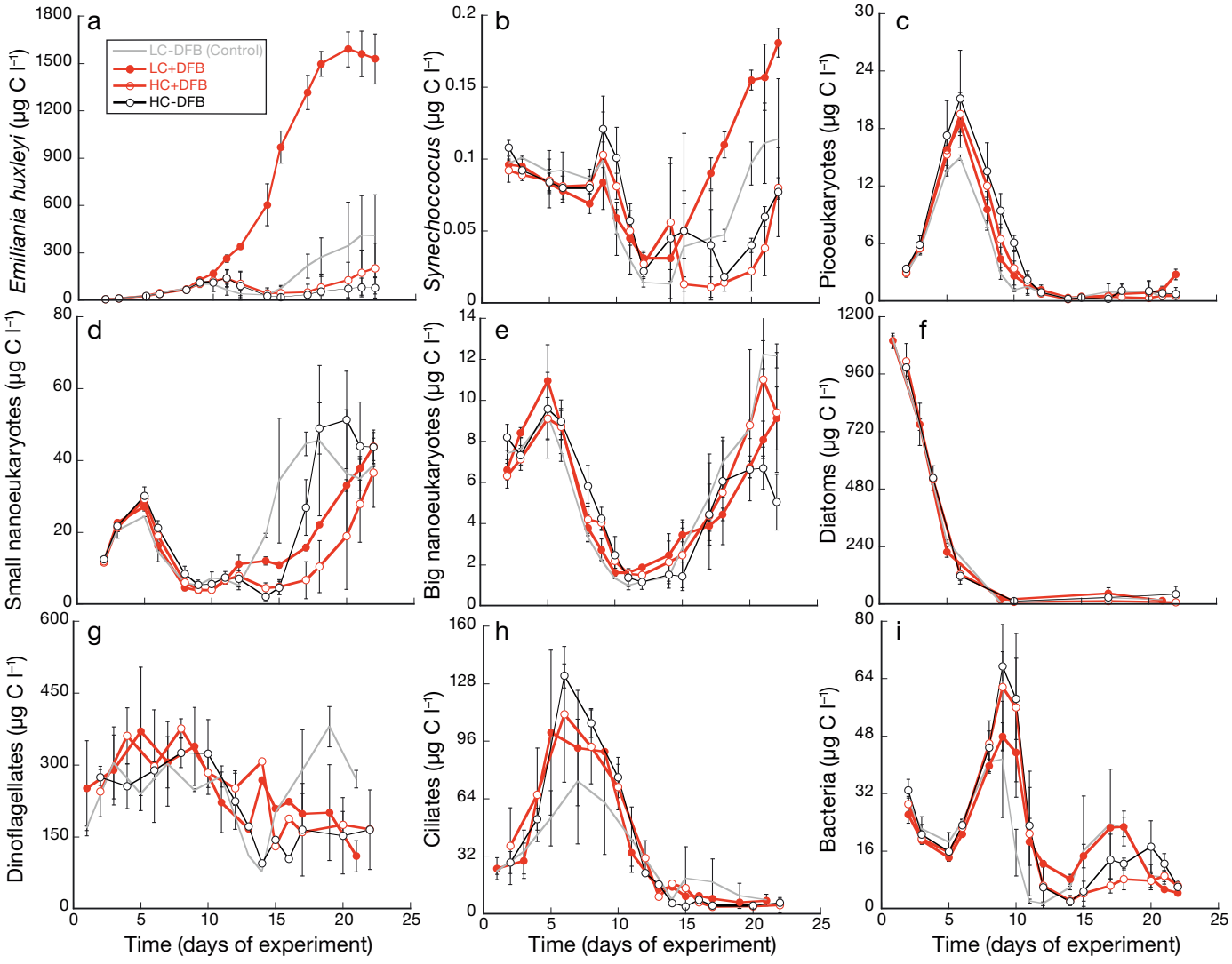

Fig. 4. Temporal development of phytoplankton, microzooplankton and heterotrophic bacterioplankton biomasses (µg C l^{-1}) in the mesocosms exposed to different CO_2 and dissolved iron (dFe) treatments. (a) *Emiliania huxleyi* (5–10 µm), (b) *Synechococcus* (0.6–2 µm), (c) picoeukaryotes (0.1–2 µm), (d) small nanoeukaryotes (prasinophytes, small haptophytes, 2–7 µm), (e) large nanoeukaryotes (small single-celled diatoms and flagellated forms, 6–20 µm), (f) diatoms (chain-forming *Skeletonema* sp. 20–>500 µm), (g) dinoflagellates (20–200 µm), (h) ciliates (20–200 µm), (i) heterotrophic bacterioplankton (0.2–0.7 µm). Symbols as in Fig. 1

huxleyi biomass was much lower in the HC treatments (200 µg C l^{-1} in HC+DFB and 78 µg C l^{-1} in HC–DFB) and remained at levels below those in the control mesocosms (400 µg C l^{-1}; Fig. 4a). Thus, the biomass of *E. huxleyi* was significantly negatively affected by pCO_2 (Sidak $p < 0.0001$) and positively by iron (Sidak $p < 0.0001$) and by the interactive effects of both factors (Sidak $p < 0.0001$). In mesocosms treated with DFB, *E. huxleyi* clearly dominated the phytoplankton biomass under low pCO_2 and high dFe conditions, with up to 9000 times higher biomass than the other groups (Fig. 4a) and faster net growth rates (up to 0.61 d^{-1}, Table 2). The 3-fold increase in dFe as a result of DFB addition produced a significant 4-fold increase in *E. huxleyi* biomass at ambient pCO_2 with respect to the control and 8- and 20-fold higher *E. huxleyi* biomasses with respect to HC+DFB and HC–DFB, respectively. In contrast, elevated pCO_2 had a negative effect on *E. huxleyi* net growth rates, inhibiting growth by 50% relative to the LC treatments (Table 2).

Synechococcus sp. showed a similar response to treatments as *E. huxleyi* (Fig. S1). After an initial decrease during phase 1, *Synechococcus* sp. recovered during phase 2 (Fig. 4b and Fig. S1b). The fastest recovery was observed in the LC treatments, with net

Table 2. Net growth rates (μ, d^{-1}) of the different groups calculated with the logistic model under the different treatments; LC: ambient CO_2 (390 μatm); HC: increased CO_2 (900 μatm); –DFB (ambient dissolved iron, dFe); +DFB (increased dFe). In the logistic model $\ln((K - N)/N)$, K is the carrying capacity, N corresponds to cell numbers at a given time, and the growth rate (μ) is the slope from the linear regression. Data are means (± SD) of 3 independent mesocosms except for the LC–DFB treatment in which n = 2. Significant differences between treatments within the same time period (i.e. 0–10 d or 11–22 d) are represented by different superscript letters (2-way ANOVA followed by post-hoc Tukey tests, where $p < 0.05$ is significant). Significant differences between the 2 time periods mentioned within the same treatment are represented by an asterisk (*t*-test). Blank spaces mean that net growth rates have non-significant determination coefficients (R^2). Note that DFB was added on Day 7

Growth rates Time period (days)	Time period (d)	μ_{LC-DFB}	μ_{LC+DFB}	μ_{HC+DFB}	μ_{HC-DFB}
Emiliania huxleyi (5–10 μm)	0–10	0.38 (0.0233)^{a*}	0.40 (0.0119)^{a*}	0.50 (0.0640)^{a*}	0.53 (0.0880)^{a*}
	11–22	0.52 (0.0571)^{a*}	0.60 (0.0009)^{b*}	0.42 (0.0545)^{c*}	0.33 (0.0073)^{d*}
Synechococcus sp (0.6–2 μm)	0–10	–	–	–	–
	11–22	0.03 (0.0645)^{a*}	0.5859 (0.0696)^{b*}	0.42 (0.0581)^{a*}	0.35 (0.0964)^{a*}
Picoeukaryotes (0.1–2 μm)	0–10	1.28 (0.0354)^{a*}	1.18 (0.1834)^{a*}	1.01 (0.0372)^{a*}	0.11 (0.0543)^{a*}
	11–22	0.33 (0.2083)^{a*}	0.14 (0.0217)^{a*}	1.15 (0.0973)^{a*}	0.08 (0.0459)^{a*}
Small nanoeukaryotes (2–7 μm)	0–10	0.20 (0.0167)^{a}	0.30 (0.0189)^{a}	0.29 (0.0077)^{a}	0.21 (0.1353)^{a}
	11–22	0.31 (0.0431)^{a}	0.32 (0.0273)^{a}	0.29 (0.1076)^{a}	0.40 (0.1166)^{a}
Large nanoeukaryotes (6–20 μm)	0–10	0.32 (0.2058)^{a}	0.41 (0.0279)^{a*}	0.28 (0.0847)^{a*}	0.31 (0.0451)^{a}
	11–22	0.40 (0.0106)^{a}	0.34 (0.0590)^{a*}	0.35 (0.0501)^{a*}	0.46 (0.0900)^{a}
Dinoflagellates (30–75 μm)	0–10	0.26 (0.0214)^{a*}	0.33 (0.0213)^{a*}	0.34 (0.2582)^{a*}	0.25 (0.0792)^{a*}
	11–22	–	–	–	–
Bacterioplankton (0.2–0.7 μm)	0–10	0.55 (0.0835)^{a*}	0.55 (0.1040)^{a*}	0.85 (0.070)^{b*}	0.99 (0.1185)^{b*}
	11–22	0.77 (0.033)^{a*}	0.72 (0.043)^{a*}	0.51 (0.1205)^{a*}	0.72 (0.2773)^{a*}

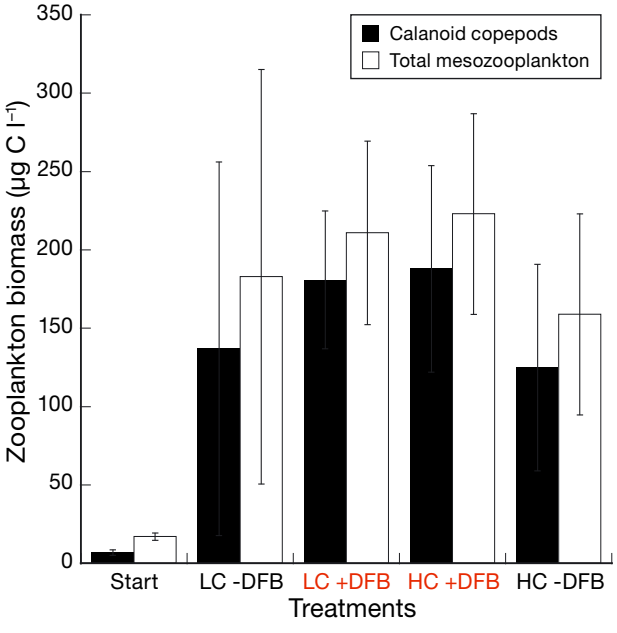

Fig. 5. Total mesozooplankton biomass (white bars) and calanoid copepods (black bars) at the beginning and at the end of the experiment. Bars indicate means of measurements in 3 independent mesocosms (n = 3) except for LC–DFB where n = 2. Error bars indicate standard deviations. Treatments and colours as in Fig. 1

growth rates of 0.58 d^{-1} and biomasses of 0.18 μg C l^{-1} in the LC+DFB mesocosms (Table 2, Fig. 4b). Elevated pCO_2 had significant negative effects on *Synechococcus* sp. from Day 12 onwards (Sidak p = 0.018 and Bonferroni $p < 0.001$). High dFe (+DFB) promoted a significant increase in biomass in the LC+DFB compared to the control (LC–DFB) from Days 14 to 22 (Sidak $p \leq 0.03$, Bonferroni $p < 0.001$) and in the growth rates (0.04 and 0.59, respectively; Table 2).

In general, biomasses and/or net growth rates of other microorganisms were not significantly affected by changes in pCO_2 and/or dFe levels or their interaction during phase 2 (all SPANOVAs, $p > 0.05$). Mesozooplankton was dominated by calanoid copepods and reached high biomass in all treatments from initially 16.5 to 159–223 μg C l^{-1} at the end of the experiment (Fig. 5), but there were no significant differences in total mesozooplankton due to the treatments (SPANOVA, $p > 0.05$).

DISCUSSION

The reproducibility between the triplicates of each treatment was high, allowing us to isolate and identify single and interactive effects on the variables

measured. The targeted high CO_2 concentrations were achieved in the 6 mesocosms, although the steady state values were slightly lower (900 µatm) than our aimed concentration (1000 µatm). However, we did not achieve a stable ambient CO_2 (LC) concentration lasting throughout the experiment. The average pCO_2 was 300 µatm and thus below the present levels. Similar difficulties were experienced by Schulz & Riebesell (2013), who reported diel variability in proton (H^+) and CO_2 concentrations during a mesocom study simulating different CO_2 scenarios ranging initially from about 370 to 1250 µatm, but dropping to 675 ± 65 and 310 ± 30 µatm by the end. A considerable natural variability exists in seawater carbonate chemistry speciation, caused by changes in temperature and biological activities such as photosynthesis, respiration, nutrient utilisation, remineralisation and calcium carbonate precipitation and dissolution (Riebesell et al. 2008, Schulz & Riebesell 2013). These processes were highly active during our experiment, mainly driven by sunny conditions during the experimental period (75% days with clear sky, 25% days with partial cloud-covered sky). Considering that variability occurs on interannual, seasonal and diurnal time scales, it forms part of the system's behaviour. However, the amplitude of these changes is predicted to increase with increasing future CO_2 levels (decreasing seawater pH) because of declining seawater buffer capacity (Schulz & Riebesell 2013).

Instead of our intention to induce Fe limitation by DFB addition on Day 7, we found that DFB enhanced dFe levels, likely due to an increase in Fe solubility. Similar results have been observed in other fjord environments (Öztürk et al. 2002). The decrease in particulate iron concomitant to the increase in dissolved iron up to a significant 12-fold change from particulate iron to dissolved iron in the LC+DFB treatment (Fig. S2 and Table S1 in the Supplement) indicates that DFB mediated the transfer of Fe from the particulate to the soluble pool. In addition, Fe solubility is enhanced at pH lower than 7.8 (Kuma et al. 1996). Hence, high CO_2 also increased dFe levels in our experiment, as previously observed in a mesocosm experiment in the same fjord (Breitbarth et al. 2010b). In conclusion, in fjord environments, dFe levels increased similarly by either the addition of CO_2 and/or DFB. Moreover, an increase in dFe by high pCO_2 (HC) in combination with DFB addition (HC+DFB) was observed, relative to the one with only high pCO_2 (HC–DFB) (Fig. 1b). This indicates that the presence of the siderophore prevented the re-precipitation of the dFe that was solubilised at high CO_2 (lower pH), and thus increased the residence time of solubilised Fe in the water column. This demonstrates a synergistic positive effect of high CO_2 and DFB on dFe concentration. To date, few investigations have examined the pH effect on iron bound to organic ligands (FeL) and Fe bioavailability. The pH effect will depend on the nature of Fe-binding functional groups of the organic ligands (Millero et al. 2009). More specifically, low pH decreases the Fe bioavailability in the presence of DFB, and has been suggested to decrease the availability of Fe within natural organic complexes (Shi et al. 2010). However, Fe-bound to some chelating agents is more photolabile at lower pH, thus likely increasing bioavailability of Fe for some FeL complexes (Sunda & Huntsman 2003). Ocean acidification has been shown to increase Fe(II) concentrations and its half-lifetime due to slower Fe(II) oxidation rates, during a mesocosm experiment in the same location as this study (Breitbarth et al. 2010b). Thus, in coastal and fjord environments, low pH and/or strong organic ligands might enhance the solubility of particulate Fe, promoting higher Fe availability to phytoplankton.

The distinct chemical conditions described above steered the mesocosms' performance into 2 clearly differentiated phases. In phase 1 (Days 0–10), ambient dFe conditions in the mesocosms were sufficient for all planktonic groups to meet their iron demand (in the range of pM, Table S2) and other macronutrients were sufficient to sustain growth (Fig. 2). Phase 1 thus consisted of a plankton succession similar to what has previously been reported (Paulino et al. 2008) with small autotrophs being grazed by microzooplankton (data not shown), which in turn were probably preyed upon by copepods (Nejstgaard et al. 2001). However, no pCO_2 effects were observed in phase 1 in any of the functional groups, except for bacterioplankton. Heterotrophic bacteria reacted positively to HC treatments towards the end of phase 1 and had higher net growth rates at increased pCO_2 levels, possibly due to enhanced available DOM, in agreement with previous studies (Endres et al. 2014) (Fig. 2). The reverse situation occurred between Days 12–18 during phase 2. This reflect changes in bacterial community composition, but further studies are needed.

In phase 2 (Days 11–22), the coccolithophore *Emiliania huxleyi*, and the cyanobacterium *Synechococcus* sp. were both affected by the different pCO_2 and Fe conditions. The effects of increased pCO_2 on *E. huxleyi* are in agreement with previous mesocosm studies (Riebesell et al. 2007) showing that elevated pCO_2 had a detrimental impact on the net growth of

E. huxleyi, while at ambient pCO_2 and high N:P ratios *E. huxleyi* dominated the phytoplankton communities (Paasche 2001). It is not surprising that *E. huxleyi* flourished under ambient CO_2 conditions due to its ability to efficiently exploit organic nutrients, to consume ammonium instead of nitrate and to use its efficient alkaline phosphatase (Fig. 2, and reflected in Paasche 2001).

However, the beneficial effect of DFB is more cryptic. Our results indicate that the DFB addition actually increased dFe, resulting in higher biomass. The insufficiency of the ambient dFe to support the *E. huxleyi* biomass can be demonstrated by calculating the iron demand of the bloom relative to the concentration of dFe in the control (LC–DFB). Our estimated Fe demand to sustain *E. huxleyi* abundance in LC+DFB was ~6–10 nM (Table S1). Values above this dFe concentration were measured in all treatments except in the control, where dFe concentrations were below 6 nM (Fig. 1b). Therefore, the cells in the control were most likely experiencing Fe limitation (i.e. the rate of dFe supply was slower than that of iron demand by the coccolithophores), which was affecting their growth rates (Table 2). In addition to slower net growth rates and reduced chl *a*, significantly lower F_v/F_m values were observed in the control with respect to the LC+DFB treatment from Days 11 to 22 (Fig. 2b). Similar low values were observed in *E. huxleyi* under Fe limitation at the same light conditions and for the same variables as in our experiment (Honey et al. 2013). This combination of symptoms is typical of Fe-deficient algae (Behrenfeld & Milligan 2013), further supporting the Fe-limited condition of *E. huxleyi in* the control. However, the observed *E. huxleyi biomass* as well as chl *a* did increase slightly in the control despite assumed iron limitation. It can be considered that dFe should decrease under these circumstances. However, Fe demand estimated for the control was 0.8 to 1 nM (data not shown). The drawdown of such iron concentration by *E. huxleyi* in the control is within the error range of our dFe measurement, thus dFe uptake by the cells might not have been evident. On the other hand, biomass can increase, and cells can still be iron limited. In this case, limited cells show slower net growth rates than Fe replete cells, as also observed by Sunda & Huntsman (1995).

Fe availability often limits primary productivity in open-ocean waters and in some coastal upwelling regions (de Baar & Boyd 2000), but Fe limitation in fjord environments is less common (Öztürk et al. 2002). Fe bioavailability depends not only on dissolved Fe concentrations, but also on Fe speciation. Although *E. huxleyi* net growth rates were higher in the LC than in the HC treatments, blooming biomass values (i.e. 60 000 cells ml^{-1}; Fig. S1) in LC were not sustained at *in situ* dFe concentrations (i.e. –DFB treatment). It can be argued that the concomitant effect of nitrate limitation occurring in the second phase (Fig. 2) and low Fe availability might have affected the dynamics of *E. huxleyi* and other plankton groups. Iron requirements of phytoplankton are strongly influenced by the availability and source of nitrogen (Maldonado & Price 1996, Schoffman et al. 2016). Phytoplankton that is using ammonium (NH_4^+) for growth has lower Fe requirements than phytoplankton using nitrate (NO_3^-; Maldonado & Price 1996, Schoffmann et al. 2016). NH_4^+ can be directly incorporated into amino acids, while extra iron is needed for nitrate assimilation, because nitrate and nitrite reductase contain Fe cofactors. In addition, the energy for NO_3 reduction is produced by the Fe-rich photosynthetic electron transport chain. In our experiment, NO_3 concentration was limiting during phase 2, but NH_4^+ increased from Day 5 to Day 15, likely as a result of remineralisation and nutrient release from the decaying diatom bloom in phase 1. Such NH_4^+ increase was sufficient to sustain growth of most phytoplankton. Given the low calculated Fe demand for the majority of phytoplankton groups in phase 2 (except for *E. huxleyi*), the dFe levels in the mesocosms were high enough to fulfil their Fe demands. In contrast, *E. huxleyi* had a high Fe demand and was thus only able to bloom in the treatments with increased dFe concentrations. The ability of *E. huxleyi* to flourish at low NO_3^- levels can be explained by its ability to efficiently use NH_4^+ and organic nitrogen sources as observed in Norwegian fjords and in the North Sea (Lessard et al. 2005). These studies further support the Fe-limited condition of the coccolithophore, because when dFe increased, the *E. huxleyi* bloom occurred despite low nitrate. In our experiment, most phytoplankton groups were not experiencing Fe limitation, which was reflected by their growth not being strongly affected by higher dFe. According to the maximum calculated biomass (Fig. 4), the N demand for each phytoplankton group was about 0.78 µM N (data not shown) (excluding *E. huxleyi* and dinoflagellates). Thus, the NH_4^+ levels measured in phase 2 (ca. 1.4 µM) were sufficient to meet their N requirements. We did not observe increases in C:chl *a* ratios (proxy for N limitation; Jakobsen et al. 2015; data not shown) during phase 2 compared to phase 1. The coccolithophore was able to use other N sources highly efficiently as mentioned above, by increasing the abundance of NH_4^+

transporters under nitrate limitation (McKew et al. 2015). Dinoflagellates were mostly heterotrophic and some mixotrophic, and in Phase 2 were dominated by *Ceratium*, which have been reported to grow under low N and P, and to use NH_4^+ and urea (Baek et al. 2008). *Ceratium* also perform luxury nitrate consumption and are able to acquire extra nutrients via phagotrophy (Baek et al. 2008), and they are large enough to escape grazing. Additionally, given that bacterial biomass increased in phase 2 again, NH_4^+ was most likely being consumed at a rate similar to the rate of organic N remineralisation.

The most remarkable result in our experiment was the massive increase in *E. huxleyi* biomass and its growth rate in the LC+DFB treatment (up to 20-fold higher biomass and 2-fold faster growth rate, Fig. 4a, Table 2). The abundance of *E. huxleyi* also increased several orders of magnitude relative to other autotrophic groups. Thus, the faster growth rates observed in the presence of DFB imply that Fe bound to DFB is bioavailable to *E. huxleyi*, as previously demonstrated by Lis et al. (2015). DFB was added in 17.5-fold excess compared to the fjord dFe concentration, therefore we assume that all dFe was complexed to DFB. Our results suggest that *E. huxleyi* is able to use DFB-bound Fe (Fe-DFB). Indeed, *E. huxleyi* produces organic complexes with high affinity for Fe (Boye & van den Berg 2000) and is able to acquire Fe from organic Fe complexes (Hartnett et al. 2012) including Fe-DFB (Shaked & Lis 2012, Lis et al. 2015). Most likely, *E. huxleyi* was able to access Fe bound to DFB by means of a reductive pathway (Maldonado & Price 2001), one of the most prevalent Fe acquisition mechanisms in phytoplankton. The fact that *E. huxleyi* biomass in the HC treatments was significantly higher in the presence than in the absence of DFB further suggests that the cells were able to cope better with the unfavourable effects of OA when they were not simultaneously Fe limited. The negative effects of OA on calcifying algae is caused by external acidification reducing the $[H^+]$ electrochemical gradient, impairing the cellular passive $[H^+]$ outflow that is a by-product of the calcification process (Taylor et al. 2012). In addition, maintaining a constant intracellular pH is energetically costly, and OA likely affects the cellular energy demands (Taylor et al. 2012). Metabolism drives traits that determine fitness, growth and survival of populations (Dell et al. 2011), thus increased dFe during our experiment may have helped the cells to meet the extra metabolic demands imposed by the decrease in pH, allowing them to sustain growth.

The response to treatments of *Synechococcus* sp. was similar to that of *E. huxleyi*, i.e. negatively affected by increased pCO_2 and positively by high dFe in the control (LC–DFB). The estimated Fe demand for *Synechococcus* sp. was ca. 2 pM (Table S2), well below the dFe concentrations in the control. This suggests that Fe concentration did not influence the net growth of *Synechococcus*. However, high dFe (+DFB) promoted a significant increase in biomass and growth rates at ambient CO_2 conditions (LC+DFB) compared to the control, indicating that higher Fe levels induced growth. Since niche differences in cyanobacteria Fe-metabolism are well documented (Desai et al. 2012), the mechanism by which the growth of *Synechococcus* is enhanced by Fe is not clear. In agreement with Paulino et al. (2008), high CO_2 led to reduced net growth and biomass in the HC treatment during phase 2. Contrasting results have been observed in another study from the Raunefjord locality (A. Larsen pers. obs.), indicating that the harmful HC effects on this species are not yet well understood. It has been hypothesised that high CO_2 might decrease photosynthetic efficiency and light saturation constants or affect nutrient availability or competition with other taxa (Mackey et al. 2015), or being perhaps more sensitive to grazing pressure. Unfortunately, we do not know at present which *Synechococcus* strains inhabit the fjord, and no molecular studies have been conducted so far to elucidate this; thus, we cannot conclude whether the increased pCO_2 and dFe effects on *Synechococcus* could be a strain-specific response, an indirect effect or the combination of both.

The consequences of the interactive effects of pCO_2 and Fe availability on *E. huxleyi* can be critical to C-cycling and marine ecosystems. Within the future predicted climate scenario for coastal ecosystems, particulate and/or colloidal iron might become more solubilised by lower pH (Sunda & Huntsman 1995, Breitbarth et al. 2010a), by natural organic ligands, and/or by increased ultraviolet radiation, which mediates photo-solubilisation (Kuma et al. 1996, Hassler & Schoemann 2009). Given the variability of responses to increased pCO_2 observed in *E. huxleyi* (Hutchins 2011, Riebesell & Tortell 2011, Meyer & Riebesell 2015), some strains that are held back by iron limitation might become more abundant, gaining a competitive advantage through their low stringent requirements for nutrients and high growth under photoinhibitory conditions (Paasche 2001) at increased Fe availability. All of these processes have a clear impact on Fe solubilisation. In coastal areas from polar regions, glacial meltwater (as a consequence of global warming) represents a significant entry of iron and colloidal matter, as well

as aerosols and riverine discharges in other coastal regions (reviewed by Marchetti & Maldonado 2016). Thus, in areas where particulate Fe inputs are important, the effectiveness of some natural chelators such as siderophores, in dissolving Fe from oxyhydroxides and/or by enhancing the photoinduced redox cycle of Fe, will be increased (Shi et al. 2010 and references therein). According to our results, the deleterious effect of OA on the development of *E. huxleyi* blooms will be more relevant in high-Fe environments than in Fe-limited ones. The loss of C production of *E. huxleyi* (estimated as the areas below the curves in Fig. 4a) due to OA was ~92% in high dFe concentration, and ~70% in control Fe conditions. The potential benefit of higher Fe availability (increased dFe levels) in an acidified ocean will be overridden by the decrease in pH itself. However, increased dFe by DFB in high-pCO_2-seawater enhanced *E. huxleyi* C production by ~60%. Fe-favoured strains of *E. huxleyi* (strains that are Fe limited under actual dFe conditions and will thrive in a high Fe environment) could outcompete other phytoplankton and influence the counterbalance between the carbonate pump and the organic carbon pump (i.e. RR, Rost & Riebesell 2004) in a future high CO_2 and high dFe ocean. RR is the ratio of particulate inorganic to organic carbon in exported biogenic matter (calcite:POC or PIC:POC), which is used as a proxy for calcification vs. photosynthesis (Hutchins 2011). In our experiment, RRs were significantly higher in LC than in HC treatments (average 0.9 vs. 0.4 respectively, Table 1), in close agreement with a number of experiments (Meyer & Riebesell 2015). Furthermore, Fe limitation has been shown to decrease PIC:POC ratios (Muggli & Harrison 1996) and $CaCO_3$ production rates (Schulz et al. 2004) in cultures of *E. huxleyi,* while the opposite has been shown under P and N limitation (Paasche 2001). PIC:POC in our study increased significantly (ca. 4-fold) during phase 2 in LC+DFB relative to all other treatments (M. R. Lorenzo et al. unpubl. data), implying that the increase in dFe might enhance calcification as observed by Muggli & Harrison (1996). Sustained growth and possibly calcification under future increased pCO_2 levels might be mediated by strains that are favoured by high dFe. If so, the PIC ballast effect in surface oceans (Sanders et al. 2010) would not be affected (calcite saturation state above 1, as shown in Table 1) and the downward POC flux would continue and directly influence the RR.

In summary, this study demonstrates that Fe concentrations can control phytoplankton community structure in coastal ecosystems and that ocean acidification can enhance Fe bioavailability. This is contrary to the idea that Fe is rarely limiting in fjord and/or estuarine environments. *E. huxleyi* was negatively affected by increased pCO_2 levels, a scenario suggested for the near future. However, our study indicates that some *E. huxleyi* strains might have higher Fe requirements than initially thought. Thus, in areas with high total Fe concentrations (particulate and dissolved Fe), the detrimental effects of increased pCO_2 on these strains can be partially mitigated by enhanced dFe, possibly inducing cascading effects on food web dynamics, carbon export and the RR. These effects will ultimately affect the exchange of CO_2 across the ocean–atmosphere interface. The interactive effects of pCO_2 and Fe observed in our mesocosm study highlight the importance of examining multiple stressors simultaneously in natural communities. Investigating how multiple drivers, competition, acclimation and adaptation interact at longer experimental times and affect natural plankton communities is essential to better predict how marine ecosystems will respond to future changes.

Acknowledgements. This work was funded by CTM/MAR 2010-17216 (Phytostress) research grant from the Spanish Ministry for Science and Innovation (Spain) to M.S. M.R.L. and C.I. were funded by FPU grants from the Ministry for Education (Spain). M.A.M. and J.A.F. were supported by Grant no. 228224, Transnational Access, from the EU FP7-INFRA-2008-1 MESOAQUA (Network of leading MESOcosm facilities to advance the studies of future AQUAtic ecosystems from the Arctic to the Mediterranean). A.L. was supported by the EU-ERC grant 250254 (MINOS) and the RCN project no. 225956/E10 (MicroPolar: Processes and Players in Arctic Marine Pelagic Food Webs — Biogeochemistry, Environment and Climate Change). We thank Jay T. Cullen for hosting M.R.L. to analyse dFe at his laboratory, Iole di Capua for counting mesozooplankton, and the Spanish Institute for Oceanography (IEO-Fuengirola, Málaga) for silicic acid analyses. We thank Jens C. Nejstgaard and Hans H. Jakobsen for discussions and suggestions, and the MBS staff for logistic support. We also thank the anonymous reviewers for helpful criticisms.

LITERATURE CITED

Baek SH, Shimode S, Shin K, Han MS, Kikuchi T (2009) Growth of dinoflagellates, *Ceratium furca* and *Ceratium fusus* in Sagami Bay, Japan: the role of vertical migration and cell division. Harmful Algae 8:843–856

Barbeau K, Rue EL, Trick CG, Bruland KT, Butler A (2003) Photochemical reactivity of siderophores produced by marine heterotrophic bacteria and cyanobacteria based on characteristic Fe(III) binding groups. Limnol Oceanogr 48:1069–1078

Behrenfeld MJ, Milligan AJ (2013) Photophysiological expressions of iron stress in phytoplankton. Annu Rev Mar Sci 5:217–246

Boye M, van den Berg CMG (2000) Iron availability and the release of iron-complexing ligands by *Emiliania huxleyi*. Mar Chem 70:277–287

Breitbarth E, Achterberg EP, Ardelan MV, Baker AR and others (2010a) Iron biogeochemistry across marine systems — progress from the past decade. Biogeosciences 7: 1075–1097

Breitbarth E, Bellerby RJ, Neill CC, Ardelan MV, Meyerh M (2010b) Ocean acidification affects iron speciation during a coastal seawater mesocosm experiment. Biogeosciences 7:1065–1073

Calbet A, Sazhin AF, Nejstgaard JC, Berger SA and others (2014) Future climate scenarios for a coastal productive planktonic food web resulting in microplankton phenology changes and decreased trophic transfer efficiency. PLOS ONE 9:e94388

Caron DA, Hutchins DA (2013) The effects of changing climate on microzooplankton grazing and community structure: drivers, predictions and knowledge gaps. J Plankton Res 35:235–252

Crain CM, Kroeker K, Halpern BS (2008) Interactive and cumulative effects of multiple human stressors in marine systems. Ecol Lett 11:1304–1315

De Baar HJW, Timmermans KR, Laan P, De Porto HH and others (2008) Titan: a new facility for ultraclean sampling of trace elements and isotopes in the deep oceans in the international Geotraces program. Mar Chem 111:4–21

De Baar HJW, Boyd PW (2000) The role of iron in plankton ecology and carbon dioxide transfer of the global oceans. In: Hanson RB, Ducklow HW, Field JG (eds) The changing ocean carbon cycle. Cambridge University Press, Cambridge, p 61–140

De Jong JTM, den Das J, Bathmann U, Stoll MHC, Kattner G, Nolting RF, de Baar HJW (1998) Dissolved iron at subnanomolar levels in the Southern Ocean as determined by ship-board analysis. Anal Chim Acta 377:113–124

Dell AI, Pawar S, Savage SM (2011) Systematic variation in the temperature dependence of physiological and ecological traits. Proc Natl Acad Sci USA 108:10591–10596

Desai DK, Desai FD, Laroche J (2012) Factors influencing the diversity of iron uptake systems in aquatic microorganisms. Front Microbiol 3:362

Doney SC, Fabry VJ, Feely RA, Kleypas JA (2009) Ocean acidification: the other CO_2 problem. Annu Rev Mar Sci 1:169–192

Dylmer CV, Giraudeau J, Hanquiez V, Husum K (2015) The coccolithophores *Emiliania huxleyi* and *Coccolithus pelagicus*: extant populations from the Norwegian-Iceland Seas and Fram Strait. Deep Sea Res I Oceanogr Res Pap 98:1–9

Egge JK, Heimdal BR (1994) Blooms of phytoplankton including *Emiliania huxleyi* (Haptophyta). Effect of nutrient supply in different N:P ratios. Sarsia 79:333–348

Endres S, Galgani L, Riebesell U, Schulz KG, Engel A (2014) Stimulated bacterial growth under elevated pCO_2: results from an off-shore mesocosm study. PLOS ONE 9: e99228

Foyer CH, Lelandais M, Kunert KJ (1994) Photooxidative stress in plants. Physiol Plant 92:696–717

Gran G (1952) Determination of the equivalence point in potentiometric titrations of seawater with hydrochloric acid. Oceanol Acta 5:209–218

Grashoff K, Erhardt M, Kremling K (1983) Methods of seawater analysis. Wiley-VCH, Weinheim

Hartnett A, Böttger LH, Matzanke BF, Carrano CJ (2012) Iron transport and storage in the coccolithophore: *Emiliania huxleyi.* Metallomics 4:1160–1166

Hassler CS, Schoemann V (2009) Bioavailability of organically bound Fe to model phytoplankton of the Southern Ocean. Biogeosciences 6:2281–2296

Hoegh-Guldberg O, Bruno JF (2010) The impact of climate change on the world's marine ecosystems. Science 328: 1523–1528

Hofmann M, Schellnhuber HJ (2009) Oceanic acidification affects marine carbon pump and triggers extended marine oxygen holes. Proc Natl Acad Sci USA 106:3017–3022

Honey DJ, Gledhill M, Bibby TS, Legiret FE and others (2013) Heme *b* in marine phytoplankton and particulate material from North Atlantic Ocean. Mar Ecol Prog Ser 483:1–17

Hutchins DA (2011) Forecasting the rain ratio. Nature 476: 41–42

Jakobsen HH, Carstensen J (2011) FlowCAM: sizing cells and understanding the impact of size distributions on biovolume of planktonic community structure. Aquat Microb Ecol 65:75–87

Jakobsen HH, Blanda E, Staehr PA, Højgård JK and others (2015) Development of phytoplankton communities: implications of nutrient injections on phytoplankton composition, pH and ecosystem production. J Exp Mar Biol Ecol 473:81–89

Kana TM, Glibert PM (1987) Effect of irradiances up to 2000 µE m^{-2} s^{-1} on marine *Synechococcus* WH7803-I. Growth, pigmentation and cell composition. Deep-Sea Res A 34:479–495

Kuma K, Nishioka J, Matsunaga K (1996) Controls on iron(III) hydroxide solubility in seawater: the influence of pH and natural organic chelators. Limnol Oceanogr 41:396–407

Langer G, Geisen M, Baumann KH, Kläs J, Riebesell U, Thoms S, Young JR (2006) Species-specific responses of calcifying algae to changing seawater carbonate chemistry. Geochem Geophys Geosyst 7:Q09006

Larsen A, Castberg T, Sandaa RA, Brussaard CPD and others (2001) Population dynamics and diversity of phytoplankton, bacteria and viruses in a seawater enclosure. Mar Ecol Prog Ser 221:47–57

Larsen JB, Larsen A, Thyrhaug R, Bratbak G, Sandaa RA (2008) Response of marine viral populations to a nutrient induced phytoplankton bloom at different pCO_2 levels. Biogeosciences 5:523–533

Lee S, Fuhrman JA (1987) Relationships between biovolume and biomass of naturally derived marine bacterioplankton. Appl Environ Microbiol 53:1298–1303

Lessard EJ, Merico A, Tyrrell T (2005) Nitrate:phosphate ratios and *Emiliania huxleyi* blooms. Limnol Oceanogr 50:1020–1024

Lis H, Shaked Y, Kranzler C, Keren N, Morel FMM (2015) Iron bioavailability to phytoplankton: an empirical approach. ISME J 9:1003–1013

Mackey KRM, Morris JJ, Morel FMM (2015) Response of photosynthesis to ocean acidification. Oceanography 28: 74–91

Maldonado MT, Price NM (1996) Influence of N substrate on Fe requirements of marine centric diatoms. Mar Ecol Prog Ser 141:161–172

Maldonado MT, Price NM (2001) Reduction and transport of organically bound iron by *Thalassiosira oceanica* (Bacillariophyceae). J Phycol 37:298–309

Malinverno E, Triantaphyllou MV, Dimiza MD (2015) Coccolithophore assemblage distribution along a temperate to

polar gradient in the West Pacific sector of the Southern Ocean (January 2005). Micropaleontology 61:489–506
Marchetti A, Maldonado MT (2016) Iron. In: Borowitzka MA, Beardall J, Raven JA (eds) The physiology of microalgae. Springer International Publishing, Cham, p 233–279
Marie D, Partensky F, Vaulot D, Brussaard CPD (1999) Enumeration of phytoplankton, bacteria, and viruses in marine samples. Curr Protoc Cytom 10:11.11.1–11.11.15
McKew BA, Metodieva G, Raines CA, Metodiev MV, Geider RJ (2015) Acclimation of *Emiliania huxleyi* (1516) to nutrient limitation involves precise modification of the proteome to scavenge alternative sources of N and P. Environ Microbiol 17:4050–4062
Menden-Deuer S, Lessard EJ (2000) Carbon to volume relationships for dinoflagellates, diatoms, and other protist plankton. Limnol Oceanogr 45:569–579
Meyer J, Riebesell U (2015) Reviews and syntheses: responses of coccolithophores to ocean acidification: a meta-analysis. Biogeosciences 12:1671–1682
Millero FJ, Woosley R, Ditrolio B, Waters J (2009) Effect of ocean acidification on the speciation of metals in seawater. Oceanography 22:72–85
Muggli DL, Harrison PJ (1996) Effects of nitrogen source on the physiology and metal nutrition of *Emiliania huxleyi* grown under different iron and light conditions. Mar Ecol Prog Ser 130:255–267
Nejstgaard JC, Naustvoll LJ, Sazhin A (2001) Correcting for underestimation of microzooplankton grazing in bottle incubation experiments with mesozooplankton. Mar Ecol Prog Ser 221:59–75
Nejstgaard JC, Frischer ME, Verity PG, Anderson JT and others (2006) Plankton development and trophic transfer in seawater enclosures with nutrients and *Phaeocystis pouchetii* added. Mar Ecol Prog Ser 321:99–121
Niehoff B, Schmithüsen T, Knüppel N, Daase M, Czerny J, Boxhammer T (2013) Mesozooplankton community development at elevated CO_2 concentrations: results from a mesocosm experiment in an Arctic fjord. Biogeosciences 10:1391–1406
Olenina I, Hadju S, Edler L, Andersson A and others (2006) Biovolumes and size classes of phytoplankton in the Baltic Sea. HELCOM Balt Sea Environ Proc 106. Baltic Marine Environment Protection Commission, Helsinki
Öztürk M, Steinnes E, Sakshaug E (2002) Iron speciation in the Trondheim Fjord from the perspective of iron limitation for phytoplankton. Estuar Coast Shelf Sci 55:197–212
Paasche E (2001) A review of the coccolithophorid *Emiliania huxleyi* (Pymnesiophyceae), with particular reference to growth, coccolith formation, and calcification-photosynthesis interactions. Phycologia 40:503–529
Paulino AI, Egge JK, Larsen A (2008) Effects of increased atmospheric CO_2 on small and intermediate sized osmotrophs during a nutrient induced phytoplankton bloom. Biogeosciences 5:739–748
Quigg A, Irwin JA, Finkel ZV (2011) Evolutionary inheritance of elemental stoichiometry in phytoplankton. Proc Biol Sci 278:526–534
Ridgwell A, Hargreaves JC, Edwards NR, Annan JD and others (2007) Marine geochemical data assimilation in an efficient Earth System Model of global biogeochemical cycling. Biogeosciences 4:87–104
Riebesell U, Gattuso JP (2015) Lessons learned from ocean acidification research. Nat Clim Chang 5:12–14
Riebesell U, Tortell PPD (2011) Effects of ocean acidification on pelagic organisms and ecosystems. In: Gattuso JP, Lansson L (eds) Ocean acidification. Oxford University Press, Oxford, p 99–121
Riebesell U, Schulz KG, Bellerby RGJ, Botros M and others (2007) Enhanced biological carbon consumption in a high CO_2 ocean. Nature 450:545–548
Riebesell U, Bellerby RGJ, Grossart HP, Thingstad F (2008) Mesocosm CO_2 perturbation studies: from organism to community level. Biogeosciences 5:1157–1164
Riebesell U, Lee K, Nejstgaard JC (2010) Pelagic mesocosms. In: Riebesell U, Fabry VJ, Hansson L, Gattuso JP (eds) Guide to best practices for ocean acidification research and data reporting. Office for Official Publications of the European Union, Luxembourg, p 95–112
Riebesell U, Gattuso JP, Thingstad TF, Middelburg JJ (2013) Arctic ocean acidification: pelagic ecosystem and biogeochemical dynamics responses during a mesocosm study. Biogeosciences 10:5619–5626
Robbins LL, Hansen ME, Kleypas JA, Meylan SC (2010) CO2calc: a user friendly carbon calculator for Windows, Mac OS X and iOS (iPhone). Open-file Rep 2010-1280. US Department of the Interior, US Geological Survey, Reston, VA
Rost B, Riebesell U (2004) Coccolithophores and the biological pump: responses to environmental changes. In: Thierstein HR, Young JR (eds) Coccolithophores: from molecular process to global impact. Springer, Heidelberg, p 99–125
Sanders R, Morris PJ, Poulton AJ, Stinchcombe MC, Charalampopoulou A, Lucas MI, Thomalla SJ (2010) Does a ballast effect occur in the surface ocean? Geophys Res Lett 37:L08602
Sarthou G, Timmermans KR, Blain S, Tréguer P (2005) Growth physiology and fate of diatoms in the ocean: a review. J Sea Res 53:25–42
Schoffman H, Lis H, Shaked Y, Keren N (2016) Iron–nutrient interactions within phytoplankton. Front Plant Sci 7:1223
Schreiber U, Schliwa U, Bilger W (1986) Continuous recording of photochemical and non-photochemical chlorophyll fluorescence quenching with a new type of modulation fluorometer. Photosynth Res 10:51–62
Schulz KG, Riebesell U (2013) Diurnal changes in seawater carbonate chemistry speciation at increasing atmospheric carbon dioxide. Mar Biol 160:1889–1899
Schulz KG, Zondervan I, Gerringa LJA, Timmermans KR, Veldhuis MJW, Riebesell U (2004) Effect of trace metal availability on coccolithophorid calcification. Nature 430: 673–676
Schulz KG, Ramos JB, Zeebe RE, Riebesell U (2009) CO_2 perturbation experiments: similarities and differences between dissolved inorganic carbon and total alkalinity manipulations. Biogeosciences 6:2145–2153
Shaked Y, Lis H (2012) Disassembling iron availability to phytoplankton. Front Microbiol 3:123
Shi D, Xu Y, Hopkinson BM, Morel FMM (2010) Effect of ocean acidification on iron availability to marine phytoplankton. Science 327:676–679
Stewart RIA, Dossena M, Bohan DA, Jeppesen E and others (2013) Mesocosm experiments as a tool for ecological climate change. Adv Ecol Res 48:71–181
Stocker TF, Qin D, Plattner GK, Tignor M and others (eds) (2013) Climate change 2013: the physical science basis. Contribution of Working Group I to the Fifth Assessment Report of the Intergovernmental Panel on Climate Change. Cambridge University Press, Cambridge

Striebel M, Kirchmaier L, Hingsamer P (2013) Different mixing techniques in experimental mesocosms— Does mixing affect plankton biomass and community composition? Limnol Oceanogr Methods 11:176–186

Sunda WG, Huntsman SA (1995) Iron uptake and growth limitation in oceanic and coastal phytoplankton. Mar Chem 50:189–206

Sunda W, Huntsman S (2003) Effect of pH, light, and temperature on Fe-EDTA chelation and Fe hydrolysis in seawater. Mar Chem 84:35–47

Taylor AR, Brownlee C, Wheeler GL (2012) Proton channels in algae: reasons to be excited. Trends Plant Sci 17: 675–684

Timmermans KR, van der Wagt B, Veldhuis MJW, Maatman A, de Baar HJW (2005) Physiological responses of three species of marine picophytoplankton to ammonium, phosphate, iron and light limitation. J Sea Res 53:109–120

Vrede K, Heldal M, Norland S, Bratbak G (2002) Elemental composition (C, N, P) and cell volume of exponentially growing and elemental composition (C, N, P) and cell volume of exponentially growing and nutrient-limited bacterioplankton. Appl Environ Microbiol 68:2965–2971

Wellburn AR (1994) The spectral determination of chlorophylls *a* and *b*, as well as total carotenoids, using various solvents with spectrophotometers of different resolution. J Plant Physiol 144:307–313

Wells ML (1999) Manipulating iron availability in nearshore waters. Limnol Oceanogr 44:1002–1008

Yoshimura T, Suzuki K, Kiyosawa H, Ono T, Hattori H, Kuma K, Nishioka J (2013) Impacts of elevated CO_2 on particulate and dissolved organic matter production: microcosm experiments using iron-deficient plankton communities in open subarctic waters. J Oceanogr 69: 601–618

Editorial responsibility: Katherine Richardson, Copenhagen, Denmark

Submitted: June 28, 2016; Accepted: December 16, 2016
Proofs received from author(s): February 2, 2017